Available online at www.easdprocedia.org
EASD Procedia EURODYN (2020) 1576-1585

EASD Procedia

EURODYN 2020
XI International Conference on Structural Dynamics
M. Papadrakakis, M. Fragiadakis, C. Papadimitriou (eds.)
Athens, Greece, 23–26 November 2020

# MOTION CONTROL PERFORMANCE OF TUNED MASS DAMPER INERTER (TMDI) IN CONTINUOUS WHITE-NOISE EXCITED CANTILEVERED BEAMS WITH VARIOUS SHAPES

**Zixiao Wang[1], Agathoklis Giaralis[2]***

[1] PhD Candidate, Department of Civil Engineering, City University of London
Northampton Square, London EC1V 0HB, UK
e-mail: Zixiao.Wang@city.ac.uk

[2] Senior Lecturer, Department of Civil Engineering, City University of London
Northampton Square, London EC1V 0HB, UK
e-mail: agathoklis.giaralis.1@city.ac.uk

**Keywords:** Tuned mass damper inerter, optimal passive vibration control, white-noise excitation, low-order modelling.

**Abstract.** The tuned mass-damper-inerter (TMDI) is a linear passive dynamic vibration absorber for motion control of dynamically excited building (primary) structures. It couples the classical tuned mass damper (TMD), comprising a secondary mass attached to the top building floor via a spring and dashpot, with an inerter, a mechanical element resisting relative acceleration, which links the secondary mass to a lower floor. Recent studies demonstrate that TMDI motion control effectiveness is influenced by the vibration modes of the uncontrolled primary structure. Herein, this influence is quantified through a parametric investigation considering a wide range of white-noise excited primary structures modelled as cantilevered continuous beams with various shapes and, therefore, different vibration modes. This quantification is facilitated by considering a low-order model of TMDI-equipped flexural cantilever which accounts for the effect of flexural rigidity and mass distribution of the primary structure as well as the influence of the fundamental mode shape to the location that the inerter connects the secondary mass to the primary structure. The investigation is further supported by optimal $H_2$ tuning of TMDI aiming to minimize the free-end primary structure displacement under white noise excitation. It is shown that the TMDI achieves enhanced structural performance as the inerter links the secondary mass further away from the top of the primary structure where the mass is attached to for all primary structure shapes. Moreover, it is found that improved TMDI performance and reduced stroke (relative secondary mass displacement with respect to the primary structure) are achieved for primary structure shapes with stiffness and mass distribution weighted heavier towards the base of the structure (i.e., when most of material is concentrated towards the bottom end of the structure) either through appropriate shaping or through increase of base to free-end depth ratio for fixed non-uniform shapes.

ISSN:2311-9020 
Peer-review under responsibility of the Organizing Committee of EURODYN 2020.
doi: 10.47964/1120.9128.20319

# 1 INTRODUCTION

In recent years the use of the inerter, defined in [1] as a mechanical element that resists relative acceleration through the inertance constant, has been widely considered in various linear passive dynamic vibration absorber configurations for enhanced motion control in dynamically excited structures [2]. Among these absorbers, the tuned mass damper inerter (TMDI) introduced in [3] attracted significant attention in the literature and its potential to achieve improved vibration suppression compared to the standard tuned mass damper (TMD) has been verified in various applications including for the seismic protection of building structures [3-5] as well as for safeguarding occupants' comfort in wind excited slender tall buildings [6-8]. In the TMDI configuration for building (primary) structures, an inerter is used to link a secondary mass attached to one building floor (commonly the top floor) through a spring in parallel with a viscous damper (dashpot) to a different (lower) floor.

Giaralis and Taflanidis [9] were the first to demonstrate for a seismically excited TMDI-equipped 10-storey shear frame structure that the more floors the inerter spans (i.e., the further lower the floor that the inerter connects the secondary mass) the more improved vibration suppression is furnished by an optimally tuned TMDI. This observation was more recently confirmed for seismically and wind excited real-life benchmark multi-storey structures [5,7]. Further, recognizing that spanning several floors may not be economically feasible in routine practical applications, Wang and Giaralis [8] proposed a local primary structure modification namely top-floor softening, which leads to an increased local difference in the primary structure mode shapes and was shown to have a similar beneficial effect with spanning more floors in wind-excited buildings equipped with a top-floor TMDI. This result suggests that the mode shapes of the uncontrolled primary structure and, hence, the mass and stiffness distribution of the primary structure influences the motion control potential of the TMDI. To this end, this paper aims to quantify this influence through a parametric investigation considering a wide range of white-noise excited primary structures modelled as cantilevered continuous beams with various shapes and, therefore, different vibration modes. This quantification is facilitated by considering a low-order model of TMDI-equipped flexural cantilever which accounts for the effect of flexural rigidity and mass distribution of the primary structure as well as the influence of the fundamental mode shape to the location that the inerter connects the secondary mass to the primary structure. The investigation is further supported by optimal $H_2$ tuning of TMDI aiming to minimize the free-end primary structure displacement under white noise excitation. The presentation starts from the definition of the simplified model and the derivation of frequency response functions used in random vibration analyses.

# 2 SIMPLIFIED 2-DOF DYNAMIC MODELLING AND ANALYSIS OF TMDI-EQUIPPED CONTINUOUS FLEXURAL CANTILEVERED BEAMS

## 2.1 Model description and equations of motion

Consider the TMDI-equipped continuous flexural cantilever beam (primary structure) depicted in Figure 1(a). The beam height is H and has distributed flexural rigidity $EI(x)$ and distributed mass $m(x)$, with $0 \leq x \leq \mathrm{H}$, while it is taken as undamped. A TMDI is attached to the free-end of the primary structure to control its lateral motion due to horizontal distributed dynamic load $p(x,t)$. Specifically, the TMDI consists of a secondary mass, $m_{TMDI}$, attached to the free-end of the primary structure through a linear spring with stiffness $k_{TMDI}$ in parallel with dashpot with damping coefficient $c_{TMDI}$ and further connected to the primary structure at height $x=\chi$ through an inerter with inertance $b$.

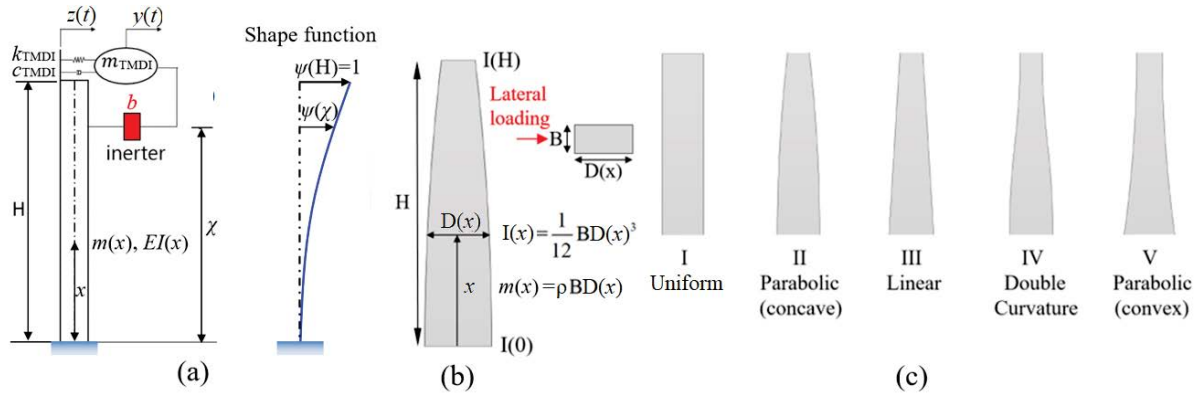


Figure 1 (a) Primary structure (cantilevered beam) equipped with TMDI and assumed mode shape, (b) Parametric variation of the primary structure, and (c) Considered primary structure geometrical shapes.

Let the lateral motion of the uncontrolled primary structure be governed by a single time-invariant shape function $\psi(x)$ which complies to the fixed support conditions at $x$=0 and, without loss of generality, is normalised such that $\psi$(H)=1 as shown in Figure 1(a). Under this assumption, the primary structure can be modelled as a generalized single degree of freedom (SDOF) system [10] and its lateral deflection can be written as $u(x,t)=\psi(x)z(t)$ where $z(t)$ is the tip displacement of the primary structure. In this setting, a simplified two degree of freedom (2-DOF) model is herein employed to approximate the lateral deflection of the TMDI-equipped cantilever beam in terms of its tip displacement $z(t)$ and the TMDI mass displacement $y(t)$ written in matrix form as

$$\mathbf{M}\ddot{\mathbf{q}}+\mathbf{C}\dot{\mathbf{q}}+\mathbf{K}\mathbf{q}=\mathbf{p}\,. \tag{1}$$

In the above equation, the displacement and forcing vectors are defined as

$$\mathbf{q}=\begin{Bmatrix} z(t) \\ y(t) \end{Bmatrix} \quad \text{and} \quad \mathbf{p}=\begin{Bmatrix} p^*(t) \\ 0 \end{Bmatrix}, \tag{2}$$

respectively, while the mass, damping, and stiffness matrix are

$$\mathbf{M}=\begin{bmatrix} m^*+b\psi(\chi)^2 & -b\psi(\chi) \\ -b\psi(\chi) & m_{TMDI}+b \end{bmatrix}, \mathbf{C}=\begin{bmatrix} c_{TMDI} & -c_{TMDI} \\ -c_{TMDI} & c_{TMDI} \end{bmatrix}, \text{and } \mathbf{K}=\begin{bmatrix} k^*+k_{TMDI} & -k_{TMDI} \\ -k_{TMDI} & k_{TMDI} \end{bmatrix}, \tag{3}$$

respectively and a dot over a symbol signifies differentiation with respect to time. Further, in the above expressions, $p^*(t)$, $m^*$, and $k^*$ are the generalized load, mass, and stiffness of the generalized SDOF representation of the primary structure defined as [Clough and Penzien 1993]

$$p^*(t)=\int_0^H p(x,t)\psi(x)dx, \quad m^*=\int_0^H m(x)\psi(x)^2dx, \quad \textit{and} \quad k^*=\int_0^H EI(x)\psi''(x)^2dx\,, \tag{4}$$

where a prime over a symbol denotes differentiation with respect to $x$.

Notably, in the herein considered 2-DOF model the assumed (single) mode shape of the primary structure, $\psi(x)$, is explicitly accounted for in defining the primary structure generalized properties in Eq.(4) as well as the inerter force through the expression

$$F_b(t)=b\left(\psi(\chi)\ddot{z}(t)-\ddot{y}(t)\right). \tag{5}$$

In the above equation, it is clearly seen that the inerter force depends on the mode shape coordinate at location $x=\chi$ (i.e., where the inerter links the attached mass to the primary structure), including the limiting case of $\psi(\chi=0)=0$ for which the inerter is grounded and the mass

matrix in Eq.(3) becomes diagonal [11]. Moreover, the 2-DOF model can also treat TMD-equipped primary structures as a special case for which $b$=0. In this regard, the 2-DOF model in Eq.(1) can be effectively used as a vehicle to study the response of TMD(I)-equipped cantilevered beams with different assumed uncontrolled dominant vibration modes as well as different inerter connecting location to the primary structure.

### 2.2 Frequency domain random vibration analysis for white noise excitation

In the ensuing numerical part of this work, three dynamic response quantities of practical interest are monitored under the assumption of uniformly distributed zero-mean spatially uncorrelated white noise excitation. These are the root mean square (RMS) values of the free-end primary structure displacement, $z(t)$, of the TMDI stroke, $z(t)$-$y(t)$ (i.e., relative displacement of the secondary mass with respect to the free-end of the primary structure), and of the inerter force in Eq.(5). These quantities are readily determined using frequency domain analysis via the expressions

$$\sigma_z = \sqrt{\int_0^{\omega_{\max}} \left| p_o^* H(\omega) \right|^2 W_o d\omega},$$

$$\sigma_{y-z} = \sqrt{\int_0^{\omega_{\max}} \left| p_o^* G(\omega) \right|^2 W_o d\omega}, \quad \text{and} \tag{6}$$

$$\sigma_{F_b} = b\sqrt{\int_0^{\omega_{\max}} \left| p_o^* B(\omega) \right|^2 W_o d\omega}.$$

In the above expressions, $\omega$ is angular frequency, $\omega_{\max}$ is a cut-off frequency above which the frequency response functions in the arguments of the integrals attain negligible values, $W_o$ is the amplitude of the white noise power spectral density function and $p_o^* = \int_0^H \psi(x)dx$ . Further, $H(\omega)$, $G(\omega)$, and $B(\omega)$ are given as

$$H(\omega) = \frac{Z(\omega)}{P^*(\omega)} = \frac{k_{22} - \omega^2 m_{22} + i\omega c_{22}}{(k_{11} - \omega^2 m_{11} + i\omega c_{11})(k_{22} - \omega^2 m_{22} + i\omega c_{22}) - (k_{12} - \omega^2 m_{12} + i\omega c_{12})(k_{21} - \omega^2 m_{21} + i\omega c_{21})},$$

$$G(\omega) = \frac{Z(\omega) - Y(\omega)}{P^*(\omega)} = \left(1 + \frac{k_{21} - \omega^2 m_{21} + i\omega c_{21}}{k_{22} - \omega^2 m_{22} + i\omega c_{22}}\right) H(\omega), \quad \text{and} \tag{7}$$

$$B(\omega) = \frac{\omega^2 \left[\psi(\chi) Z(\omega) - Y(\omega)\right]}{P^*(\omega)} = \omega^2 \left[\psi(\chi) + \frac{k_{21} - \omega^2 m_{21} + i\omega c_{21}}{k_{22} - \omega^2 m_{22} + i\omega c_{22}}\right] H(\omega),$$

respectively, where $i = \sqrt{-1}$ , and $m_{mn}$, $c_{mn}$ and $k_{mn}$, with m,n=1,2 are the elements of the matrices in Eq. (3).

## 3 OPTIMAL TMDI DESIGN USING THE SIMPLIFIED 2-DOF MODEL

To support meaningful discussion on motion control performance of TMDI-equipped structures, it is deemed essential to optimally design/tune the TMDI to minimize primary structure response. To this aim, an optimization problem is formulated to tune TMDI stiffness and damping properties such that the RMS displacement of the primary structure free-end under white noise excitation, taken as the objective function (OF), is minimized. That is,

$$\text{OF}=\sigma_z \,. \tag{8}$$

The design problem has 5 non-dimensional design variables (DVs), namely the inerter connectivity ratio CR, the mass ratio $\mu$, the inertance ratio $\beta$, the TMDI frequency ratio $\upsilon_{TMDI}$, and the TMDI damping ratio $\xi_{TMDI}$ defined as

$$\text{CR}=\frac{\text{H}-\chi}{\text{H}},\quad \mu=\frac{m_{TMDI}}{m^*},\quad \beta=\frac{b}{m^*},\quad \upsilon_{TMDI}=\frac{\sqrt{\frac{k_{TMDI}}{(m_{TMDI}+b)}}}{\omega_1},\ \text{and}\ \xi_{TMDI}=\frac{c_{TMDI}}{2\sqrt{(m_{TMDI}+b)k_{TMDI}}}, \tag{9}$$

where $\omega_1$ is the first natural frequency of the uncontrolled primary structure. Then, optimal primary DVs, $\upsilon_{TMDI}$ and $\xi_{TMDI}$, are sought that minimize the OF given values of the secondary DVs: CR, $\mu$, and $\beta$. The optimization problem is numerically solved in the ensuing numerical work using a pattern search algorithm [12] with iteratively updated search range of the primary variables hard-coded in MATLAB®.

## 4 PERFORMANCE ASSESSMENT OF TMDI-EQUIPPED CANTILEVERED BEAMS WITH DIFFERENT GEOMETRIC SHAPES

### 4.1 Parametric variation of primary structure geometric shape

As seen in section 2, the dominant vibration mode of the uncontrolled primary structure $\psi(x)$ enters explicitly in the definition the generalized primary structure properties as well as in the mass matrix of the simplified 2-DOF model used to capture the response of TMDI-equipped cantilevered beams. Given that in many practical applications the first mode, $\varphi_1(x)$, of the primary structure dominates its dynamic response, the choice of $\psi(x)= \varphi_1(x)$ is meaningful. However, $\varphi_1(x)$ depends heavily on the stiffness (flexural rigidity) and mass distribution along the height of the primary structure. To this end, the influence of the dominant vibration mode to the motion control potential of the TMDI is herein studied by varying parametrically the geometric shape (profile) of the primary structure as shown in Figure 1(b). Specifically, primary structures with fixed width $B$ along the height of the structure but varying depth $D(x)$ within the direction of the lateral load are considered which further influence the flexural rigidity and mass distribution as specified in Figure 1(b). The five different primary structure shapes plotted in Figure 1(c) are considered. Shape I (uniform) has constant cross-section along the primary structure height and slenderness ratio H/D= 20, whereas two different depth ratios defined as R=D(0)/D(H), i.e., R=2 and R=5, are considered for the remaining four non-uniform shapes. Importantly, all 9 considered primary structures have the same total area/volume and, thus, total mass which is taken as a practical reference criterion in the herein undertaken comparative study.

### 4.2 Numerical derivation of fundamental mode shapes and optimal TMDI tuning

The fundamental mode shape of each of the 9 in total different uncontrolled primary structures herein considered is obtained numerically using finite element (FE) discretization. Specifically, each primary structure is discretized using 40 tapered equal-length beam elements. A 41-DOF planar dynamic system is then derived involving only one lateral translational DOF per FE node grid along the horizontal load direction in terms of a diagonal mass matrix and a full stiffness matrix. The mass matrix is formed by lumping the own-mass of the elements at the nodes while the stiffness is constructed using standard static condensation to eliminate vertical and rotational DOFs at each FE node. Next, standard modal analysis is conducted to obtain the first mode shape vector with 41 elements. The central difference method is used to obtain the second derivative of the fundamental mode shapes. Next, the standard trapezoid quadrature rule is used to calculate the integrals defining the generalized primary structure properties in Eq.(4) for each of the 9 primary structures. Finally, the optimization problem described in section 3 is solved to find optimal $k_{TMDI}$ and $c_{TMDI}$ from the non-dimensional frequency and damping ratios in Eq.(9) for each primary structure. Given that the focus of this paper is to investigate the influence of mode shapes to TMDI performance, fixed values for the mass ratio and inertance ratio are herein assumed taken equal to $\mu$= 0.1% and $\beta$=16% and the average generalised mass from all 13 primary structures is used in the numerator of these ratios in Eq.(9). However, the CR in Eq.(9) is parametrically investigated as its influence is coupled with the influence of the fundamental mode shape through the modal coordinate $\psi(\chi)= \varphi_1(\chi)$ affecting the mass matrix of the mode in Eq. (3). In this regard, CR is let to vary within the range [0 1], where CR=1 corresponds to grounded inerter ($\chi$=0).

### 4.3 Influence of depth ratio R

The influence of fundamental mode shape variation due to different depth ratio R=D(0)/D(H) values of the primary structure to the TMDI motion control potential is firstly investigated. This is facilitated by plotting the RMS free-end displacement of optimal TMDI-equipped primary structures against CR for fixed R separately for each of the geometric shapes II-V of Figure 1(c). These plots are presented in Figure 2 where the free-end TMDI-equipped primary structure displacement is normalized by the corresponding TMD-equipped primary structure obtained by solving the optimization problem in section 3 for $b$=0. In all plots the same R=1 curve corresponding to the uniform section shape (I) is included as a base-line.

It is evidenced that improved vibration suppression is achieved, though at a decreasing rate, as CR increases (i.e., as the further away from the free-end the inerter links the secondary mass to the primary structure) irrespective of the geometric shape and, thus, the mode shape of the primary structure. Further, for relatively small CR values the TMD outperforms the TMDI. These results agree with previous numerical studies addressing different structures and dynamic loads [4,5,7] which confirms the validity of the herein considered simplified 2-DOF model for optimal TMDI design. More interestingly, it is seen that for all the considered primary structure shapes TMDI performance improves as the depth ratio increases for any fixed CR and this improvement is more substantial for lower CR values. This observation suggests that the TMDI becomes more effective in mitigating lateral vibrations in cantilevered beam-like primary structures (such as tall buildings, and chimneys) as their upper part becomes more flexible through upwards tapering. In this regard, the critical CR value for given host structure geometric shape and inertial TMDI parameters (i.e., mass $m_{\text{TMD}}$ and inertance $b$), that needs to be exceeded for TMDI to outperform TMD depends heavily on the depth ratio R. For instance, for double curvature shape (IV) shown in Figure 2(c), the critical CR values are 7.4%, 5.1%, and 2.75% for

depth ratios R 1, 2, and 5, respectively. Hence, the requirement to the inerter span reduces as the primary structure tapering rate towards reduced cross-section with height increases.

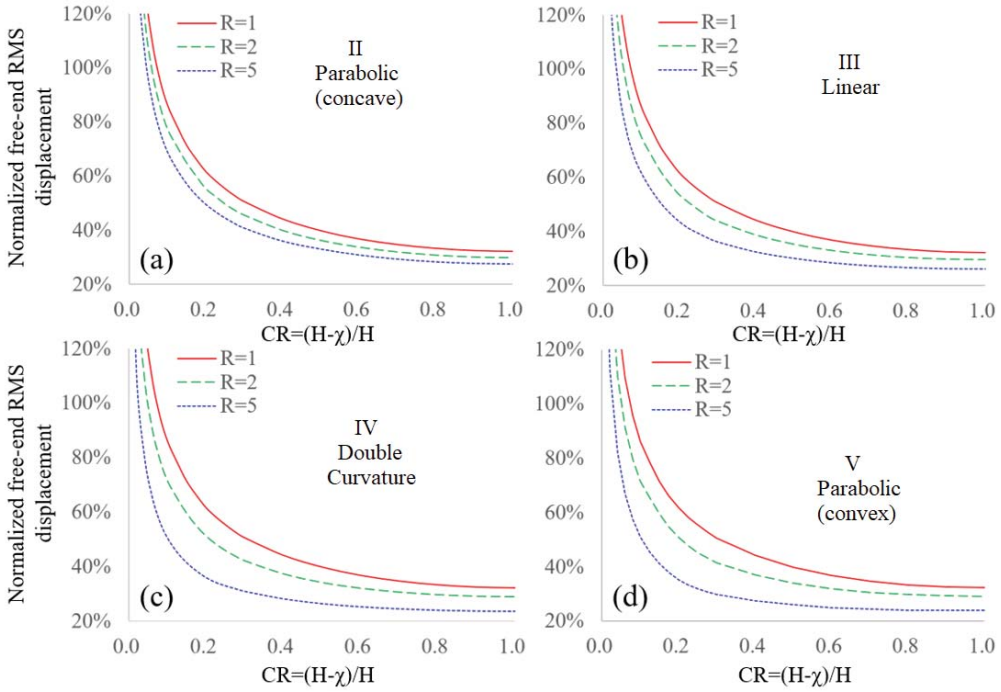


Figure 2. Free-end RMS displacement performance of optimal TMDI-equipped primary structures as function of the inerter connectivity ratio (CR) for various depth ratios R=D(0)/D(H).

### 4.4 Influence of depth profile D (primary structure shape)

Here, attention is firstly focused on exploring the influence of fundamental mode shape variation due to different primary structure shaping (see Figure 1(c)) to the TMDI motion control potential. This is facilitated by bar-plotting the RMS free-end displacement of TMDI-equipped primary structures with different shapes for CR=2.5%, 5.0%, and 7.5%, and for all different depth ratios in the upper row of panels in Figure 3. The same normalization of the RMS displacement as in Figure 2 applies. A consistent trend in these plots appears: the TMDI motion control potential increases for fixed CR and R as the primary structure shape changes from type "II" towards type "V". With reference to the shapes in Figure 1(c), this trend ultimately confirms again that better TMDI motion control is achieved as mass and stiffness distribution is heavier weighted towards the fixed-end of the primary structure. Interestingly, worst performance is noted for uniformly distributed mass and stiffness. For example, for depth ratio R=2 and CR= 5.0%, the TMDI with $\beta$=16% achieves gradually improved performance compared to the TMD by 0.5%, 2.7%, 4.7%, and 5.3% for primary structure shapes II, III, IV, and V respectively. As discussed before, for the relatively low CR=2.5% value in Figure 3(a), the TMD always outperforms the TMDI, but as CR increases (compare e.g. Figure 3(b) with 3(c) and note the difference in the y-axis scale) improvement of TMDI versus TMD become more substantial. The improved TMDI performance as the upper part of primary structure becomes more flexible is readily attributed to smaller values of $\psi(\chi)$ as the mode shape curvature increases (i.e., as the difference of $\psi$(H)- $\psi(\chi)$ increases). Nevertheless, the improvement achieved through increase of R is less significant for shapes II and III compared to shapes IV and V. This

result demonstrates that careful design/shaping of the primary structure is required to achieve increased TMDI control performance.

Moreover, the second row of panels in Figure 3 furnishes bar-plots of RMS stroke values $\sigma_{y-z}$ computed from Eq.(6) for the same cases as the first row of panels of Figure 3 and normalized by the RMS stroke for the TMD. As has been reported in several previous studies [6,7], the inclusion of the inerter to the TMD reduces dramatically the secondary mass stroke (relative displacement of secondary mass with the primary structure free-end) with higher reductions achieved as CR increases. For all the herein considered primary structures and CRs, the reduction is more than 80%. Here, a novel observation is that mode shape differences due to either the shape of the primary structure or its depth ratio do not influence as much the stroke as they influence the free-end displacement. Still, it is important to note that stroke demands follow consistently the same reduction trend as free-end displacement demand with mode shape variation: as R increases for the same primary structure shape or as shapes go from type II to type V for fixed R the normalized stroke reduces by about 1% irrespective of the CR. This is a quite welcoming result as stroke is proportional to TMDI cost in several practical applications [5,6].

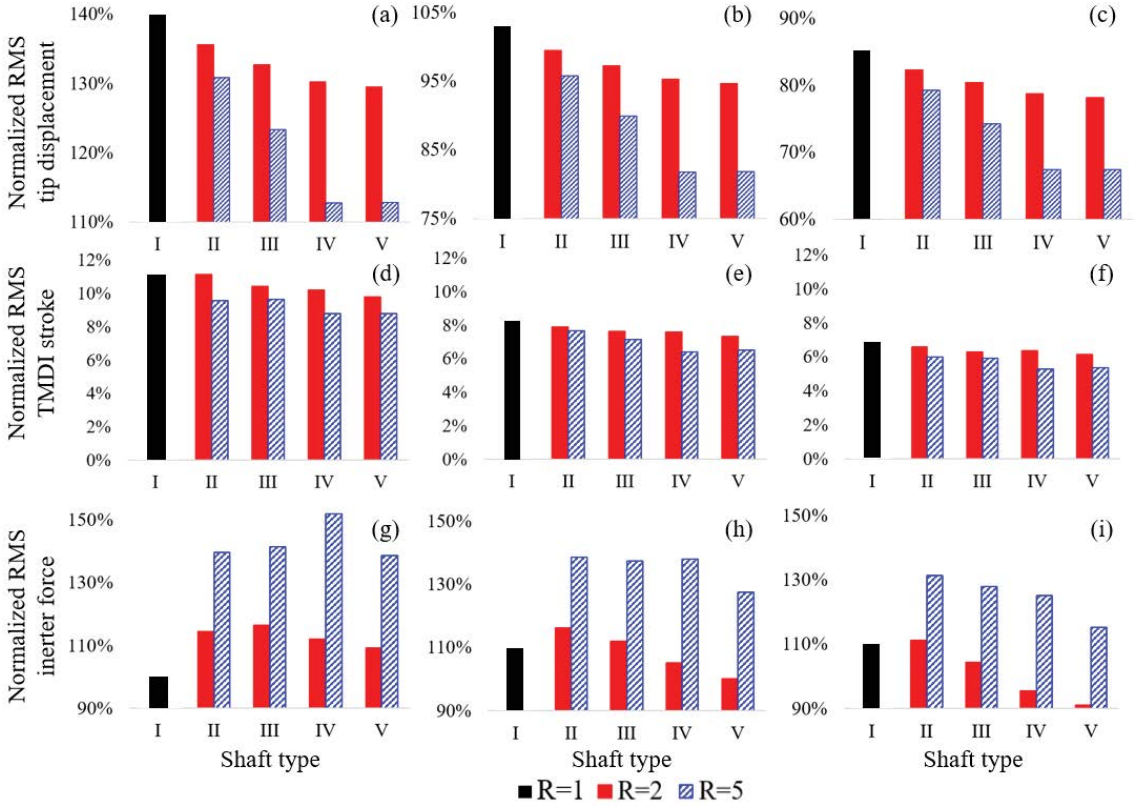


Figure 3. Free-end RMS displacement performance (upper panels), RMS TMDI stroke performance (middle panels) and RMS inerter force (lower panels) for different primary structure shape, depth ratio R and connectivity ratio CR. Values in the first two rows of panels are normalized with respect to TMD case (b=0) and values in the last row of panels are normalized with the respect to R=1, CR=2.5% TMDI case.

Lastly, considering that modal information affects explicitly the magnitude of the inerter force exerted to the primary structure at x=$\chi$ location, it is deemed practically important to gauge the influence of mode shapes variation to the inerter force in the last row of panels of Figure 3. In these plots, inerter force values are normalized by the inerter force developing at the uniform cantilever with CR=2.5%. Interestingly, it is seen that lower force develops at the uniform shaped primary structure compared to all the other shapes for the relatively large depth ratio

R=5. On the other hand, inerter force decreases for R=2 and 5 as shapes vary from type II to type V for relatively large CRs, e.g., CR=5.0% and 7.5%. One may be tempted to interpret this decrease of inerter force as the cause of TMDI achieving improved vibration suppression with primary structure shape variation seen in the first row of panels in Figure 3. However, this trend changes for a given primary structure shape with increasing depth ratio R: inerter force increases significantly as R increases from 2 to 5 for all primary structure shapes considered. Thus, the inerter force is not necessarily consistent with TMDI performance in terms of free-end displacement which, ultimately, is mostly related to the control force exerted at the free-end of the cantilever through the spring and dashpot. However, with reference to the upper row of panels in Figure 3, the increase in inerter force is accompanied with enhanced TMDI performance through increasing the depth ratio R. In this respect, it can be concluded that modifying the primary structure fundamental mode shape through more elaborate primary structure shaping rather than through increasing the depth ratio R is more advantageous in enhancing TMDI performance as it does not lead to increased inerter force exerted at the primary structure.

## 5 CONCLUDING REMARKS

The influence of the geometric shape of cantilevered primary structures to the TMDI performance for suppressing vibrations due to white noise external loading has been parametrically investigated. Five different shapes of primary structure have been considered with different base to free-end depth ratio with a TMDI attached to their free-end. Parametric analysis has been facilitated by a simplified 2-DOF in which the primary structure is represented by a generalized SDOF system whose properties account for the geometric shape of the structure through the mass and stiffness distribution along the structure height as well as through the fundamental mode shape of the structure. Further, the adopted 2-DOF model explicitly accounts for the location of the primary structure to which the inerter links the secondary mass. Since the primary structure modal coordinate at this location multiplies the inertance and depends on the shape on the shape of the primary, the inerter connection location was also varied in the parametric investigation. TMDI performance has been evaluated in terms of RMS free-end displacement for which the TMDI was optimally tuned. It is found that TMDI performance improves monotonically but at a reduced rate as the inerter connecting location to the primary structure moves away from the free end for all nine different primary structure shapes. Moreover, it was shown that improved TMDI performance as well as stroke are achieved for primary structure shapes with stiffness and mass distribution weighted heavier towards the base of the structure (i.e., when most of material is concentrated towards the bottom end of the structure) either through appropriate shaping or through increase of base to free-end depth ratio for fixed shape. Lastly, numerical data suggest that the primary structure shaping (i.e., considering more "pointy" primary structure geometry/shape) is practically most beneficial as it does not create increased inerter force exerted to the primary structure. Overall, the herein investigation point to the importance of primary structure design to enhance the dynamic performance of optimal TMDI-equipped structures.

## REFERENCES

[1] M.C. Smith, Synthesis of Mechanical Networks: The Inerter, *IEEE Transactions On Automatic Control* 47(10), 1648-1662, 2002.

[2] A.A. Taflanidis, A. Giaralis, D, Patsialis, Multi-objective optimal design of inerter-based vibration absorbers for earthquake protection of multi-storey building structures, *Journal of the Franklin Institute* 356, 7754-7784, 2019.

[3] L. Marian, A. Giaralis, Optimal design of inerter devices combined with TMDs for vibration control of buildings exposed to stochastic seismic excitations, *Proc,.11th ICOSSAR Int. Conf. on Structural Safety and Reliability*, 1025-1032, 2013.

[4] A. Giaralis, A.A. Taflanidis, Optimal tuned mass-damper-inerter (TMDI) design for seismically excited MDOF structures with model uncertainties based on reliability criteria, *Struct. Control Health Monit.* 25, e2082, 2018.

[5] R. Ruiz, A.A. Taflanidis, A. Giaralis, D. Lopez-Garcia, Risk-informed optimization of the tuned mass-damper-inerter (TMDI) for the seismic protection of multi-storey building structures, *Eng. Struct.* 177, 836-850, 2018.

[6] A. Giaralis, F. Petrini, Wind-induced vibration mitigation in tall buildings using the tuned mass-damper-inerter (TMDI), *J. Struct. Eng.*, DOI: 10.1061/(ASCE)ST.1943-541X.0001863, 2017.

[7] F. Petrini, A. Giaralis, and Z. Wang, Optimal tuned mass-damper-inerter (TMDI) design in wind-excited tall buildings for occupants' comfort serviceability performance and energy harvesting, *Eng. Struct.* 204, 109904, 2020.

[8] Z. Wang, A. Giaralis, Top-storey softening in optimal tuned mass damper inerter (TMDI)-equipped wind-excited tall buildings for enhanced serviceability performance under vortex shedding effects, *J. Struct. Eng.*, DOI: 10.1061/(ASCE)ST.1943-541X.0002838, 2020.

[9] A. Giaralis, A.A. Taflanidis, Reliability-based design of tuned-mass-damper-inerter (TMDI) equipped stochastically support excited structures, *In: Proceedings of the 12th International Conference on Applications of Statistics and Probability in Civil Engineering- ICASP12*, 2015.

[10] R.W. Clough, J. Penzien, *Dynamics of Structures*, ISBN-13: 978-8123926636, 1993.

[11] L. Marian, A. Giaralis, Optimal design of a novel tuned mass-damper–inerter (TMDI) passive vibration control configuration for stochastically support-excited structural systems. *Prob. Eng. Mech.* 38, 156–164, 2014.

[12] A. Charles, J.E. Dennis Jr., Analysis of Generalized Pattern Searches, *SIAM Journal on Optimization* 13(3), 889–903, 2003.